Check for updates

Wastewater depollution of textile dyes and antibiotics using unmodified and copper oxide/zinc oxide nanofunctionalised graphene oxide materials†

Piumie Rajapaksha, [ID] [a] Rebecca Orrell-Trigg, [ID] [a] Yen B. Truong, [ID] [b] Daniel Cozzolino, [c] Vi Khanh Truong [ID] *[a] and James Chapman [ID] *[a]

Textile dyes and pharmaceutical discharges are playing a major role as wastewater contaminants, with serious impacts on both the environment and individuals' health and wellbeing. In this article, graphene oxide was produced by oxidising graphite following a modified Hummers method, which then formed a platform to make two composite materials, copper oxide-reduced graphene oxide (CuO-rGO) and zinc oxide-reduced graphene oxide (ZnO-rGO). These materials' adsorption capacity for textile dyes rhodamine-6G (R-6G) and malachite green (MG), and antibiotic pharmaceuticals amoxicillin (AMOX) and tetracycline (TC) was analysed using a UV-visible spectroscopic method. GO showed an adsorption capacity of 625 mg g^{-1} and 813 mg g^{-1} for removing R-6G and MG dyes at pH 7 and 333 K, with a 99% regeneration efficacy and <90% reuse after 5 recycle experiments. CuO-rGO provided the highest antibiotic removal of 405 mg g^{-1} and 552 mg g^{-1} for AMOX and TC, at pH 7 and 333 K, with an 80% regeneration efficacy and 82% reuse after 5 recycle experiments. The adsorption process of R-6G, MG, AMOX and TC on GO, CuO-rGO and ZnO-rGO materials confirmed the Langmuir adsorption isotherm and pseudo-second order kinetic equations, suggesting chemisorption adsorption processes. A thermodynamic analysis indicated that each adsorption process is spontaneous. The R-6G and MG adsorption on GO, CuO-rGO and ZnO-rGO was endothermic and the AMOX and TC antibiotic adsorption on CuO-rGO and ZnO-rGO was exothermic, while the AMOX and TC adsorption on GO was endothermic as identified by the thermodynamic analysis. Chemical changes in the nanomaterials were observed after adsorption of dye and antibiotics using an attenuated total reflectance Fourier transform mid-infrared (ATR-FTIR) spectroscopic method. The hydroxyl and carbonyl functional groups were typical of GO material characterisation, which efficiently removed the cationic dye molecules. The reduced-GO materials efficiently removed the anionic antibiotic molecules from water. The plausible adsorption mechanisms are electrostatic interactions and $\pi-\pi$ interactions between the dye and antibiotic molecules and the adsorbent materials. The study demonstrates that unmodified GO can be used as an efficient adsorbent for removing cationic contaminants and the reduced-GO materials effectively remove anionic contaminant molecules from wastewater systems.

Environmental significance

The sources, fates, and transfer of cationic or anionic emerging contaminants pose a severe water pollution problem in the wastewater industry. The most significant sources of these compounds are usually anthropogenic and through discharges from industry, meaning new removal methods are essential. The work generates hybrid nanofunctional ZnO and CuO graphene oxide materials, which show the removal and kinetics of removal for antibiotics and dyes in a fundamental paper. We show that nanofunctional hybrid materials are a promising selective sorbent for the chemicals we tested. This work can potentially change membrane composition for water depollution applications and provide significantly fundamental adsorption data for other researchers to understand the uptake/removal ability.

[a]*School of Science, RMIT University, 124 La Trobe St., Melbourne, VIC 3000, Australia. E-mail: james.chapman@rmit.edu.au*

[b]*CSIRO Materials Science and Engineering, Commonwealth Scientific and Industrial Research Organization (CSIRO), Clayton, Victoria 3168, Australia*

[c]*Centre for Nutrition and Food Sciences, The University of Queensland, St. Lucia, Brisbane, QLD 4069, Australia*

† Electronic supplementary information (ESI) available. See https://doi.org/10.1039/d2va00059h

1 Introduction

Discharging large volumes of harmful chemical waste in water effluents including textile dyes and antibiotics has become a serious global issue affecting the environment, aquatic organisms, biodiversity, and the health of people.[1–3] Commonly

used textile dyes malachite green (MG) and rhodamine-6G (R-6G) are harmful chemicals with high toxicity posing terato-genic, carcinogenic, and mutagenic health problems.[4–6] These aromatic dye molecules cannot be easily eliminated from wastewater systems, and can thus be detected in surface water affecting the surrounding aquatic biota.[7,8] These dye molecules also give a colour to the water body, decreasing light penetration, and thus reducing the rate of photosynthesis.[4,9] As a result, the levels of dissolved oxygen will decrease leading to the death of aquatic organisms due to formation of an anoxic environment.[10] The improper disposal, overuse and misuse of dyes and antibiotics is therefore a common wastewater issue.[11] Additionally, freely available antibiotic molecules in the water system have caused subsequent issues such as antimicrobial resistance (AMR) in waterborne pathogens.[12] These 'AMR superbugs' have potential to spread waterborne diseases that are difficult to detect and treat.[13]

Existing wastewater treatment methods including traditional and biological methods to remove dyes and pharmaceuticals are inefficient, due to the persistent nature and non-biodegradability of these contaminants.[14,15] Therefore, novel wastewater treatment technologies and methods utilizing novel materials are highly sought after by the water sector for the removal of toxic chemicals in an eco-friendly, fast, and sustainable manner.[16,17] Highly efficient and low cost wastewater purifying technologies would also make a vast difference to developing nations where highly contaminated water sources are known to exist, but these countries are unable to afford advanced technologies.[18,19]

Current wastewater treatment technologies include oxidation, photocatalytic, electrolytic, and biological methods, micro/nano/ultra-filtration and adsorption.[20–23] Among them, adsorption is the most feasible, economic, and efficient technology to remove the water soluble toxic chemicals.[20,24] Many natural and synthetic adsorbents such as clay, charcoal, zeolite, activated carbon, bio-polymers, hydrogels, metal–organic framework membranes and MXene nanomaterials have been introduced and used in wastewater remediation.[20,25–31] Among them, carbon based adsorbents have been used as they are highly efficacious for the adsorption of organic chemicals from wastewater systems.[32] Highly efficient carbon adsorbents have evolved in recent years, with the emergence of advanced carbon nano-materials including the development of carbon nanotube, fullerene and graphene based technologies.[33] Graphene based materials, including graphene oxide (GO), reduced-GO (rGO), and chemically functionalised-GO, are considered to have favourable properties towards adsorption.[6,21,34] GO typically has a plethora of oxygen functional groups such as carboxyl, hydroxyl, and epoxy on the material's planes and edges; these functional groups have made GO a highly adsorbing and thus chemical removing material.[35,36]

GO and other composite metal based GO materials such as CuO and ZnO metal nanoparticle doped GO materials (GO, CuO-GO and ZnO-GO) have proven to be excellent antimicrobial materials, killing waterborne pathogens.[37–39] If these nanomaterials could also eliminate textile dyes and pharmaceuticals, these materials could be identified as next-generation

pathogen-killing and chemical-removing materials from more complex wastewater systems. This dual-material property will lead to the reduction of harsher chemical disinfection methods at the tertiary treatment stages of wastewater treatment before releasing contaminated effluents into surface waters. The present study fabricated the GO material by oxidising and exfoliating raw graphite, following a modified Hummers method. This synthesised GO was doped with CuO and ZnO to produce copper oxide-reduced GO (CuO-rGO) and zinc oxide-reduced GO (ZnO-rGO). The aim of the study was to identify the most suitable adsorbents to remove textile dyes and antibiotics from wastewater. These three nanomaterials were evaluated for their adsorption efficacy of textile dyes (R-6G and MG) and antibiotics (AMOX and TC), also investigating the effect of temperature, pH, adsorbent dosage and contact time with the synthesised composite adsorbents. The adsorption experiments examined the kinetics, adsorption isotherms, thermodynamic parameters, regeneration, and reusability potential of the material. The changes of chemical entities on the GO, CuO-rGO and ZnO-rGO were qualitatively analysed after the adsorption of
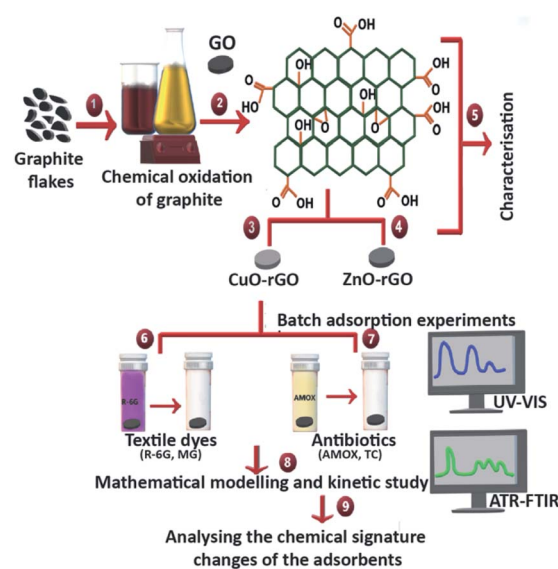

Fig. 1 Schematic of the experimental design. (1) Synthesising graphene oxide (GO) from oxidising raw graphite flakes using a modified Hummers method. (2) Resulting GO. (3) Synthesising copper oxide doped reduced-graphene oxide (CuO-rGO) using synthesised GO and $CuSO_4 \cdot 5H_2O$ aqueous solution and (4) synthesising zinc oxide doped reduced-graphene oxide (ZnO-rGO) using synthesised GO and $ZnSO_4 \cdot 7H_2O$ aqueous solution following a series of thermal chemical reactions. (5) Chemical and physical characterisation of GO, CuO-rGO and ZnO-rGO using standard microscopic and spectroscopic instruments SEM, TEM, ATR-FTIR and XPS. (6) Batch adsorption experiments of textile dyes rhodamine 6G (R-6G) and malachite green (MG) and (7) antibiotics amoxicillin (AMOX) and tetracycline (TC) from aqueous solutions using GO, CuO-rGO and ZnO-rGO adsorbents following UV-vis spectroscopy analyses. (8) Applying mathematical modelling and kinetics to study the batch adsorption of textile dyes (R-6G, MG) and antibiotics (AMOX, TC) on the GO, CuO-rGO and ZnO-rGO. (9) Analysing functional group changes on the GO, CuO-rGO and ZnO-rGO adsorbents after the adsorption of textile dyes and antibiotics using ATR-FTIR.

© 2022 The Author(s). Published by the Royal Society of Chemistry

Environ. Sci.: Adv., 2022, **1**, 456–469 | **457**

dyes and antibiotics on each adsorbent following an ATR-FTIR spectroscopic method (Fig. 1).

2 Experimental

2.1 Materials

All chemicals were reagent grade and used without further purification. The materials used in this study were as follows: graphite flakes (Sigma-Aldrich Australia), 98% sulphuric acid (Sigma-Aldrich Australia), 99% sodium nitrate (Sigma-Aldrich Australia), 99% potassium permanganate (Sigma-Aldrich Australia), Milli-Q water (18.0 μΩ cm), 30% hydrogen peroxide (Sigma-Aldrich Australia), 37% hydrochloric acid (Sigma-Aldrich Australia), 97% sodium hydroxide (Sigma-Aldrich Australia), 99% zinc sulphate heptahydrate (Sigma-Aldrich Australia), 99% copper sulphate pentahydrate (Sigma-Aldrich Australia), 98% sodium borohydride (Sigma-Aldrich Australia), rhodamine-6G (Sigma-Aldrich Australia), malachite green (Sigma-Aldrich Australia), amoxicillin (Sigma-Aldrich Australia), tetracycline hydrochloride (Sigma-Aldrich Australia), sodium carbonate (Sigma-Aldrich Australia), 98% chloramine-T trihydrate (Sigma-Aldrich Australia), and silicon wafers. Milli-Q (M.Q.) water was prepared using an ultrapure water system with a resistivity of 18.0 μΩ cm (Millipak Express 20).

2.2 Synthesis of GO nanomaterial

GO was synthesised by oxidising raw graphite flakes using a modified Hummers method.[40] The graphite flakes (3 g) were mixed with concentrated sulphuric acid (70 mL), and sodium nitrate (1.5 g) and the whole mixture was continuously stirred in an ice bath at <4 °C for 30 min. Potassium permanganate (9 g) was added into the mixture using a small spatula (*ca.* 0.1 g) followed by stirring for another 24 h achieving complete oxidation of the graphite. The mixture was diluted with M.Q. water (250 mL followed by another 150 mL) followed by the addition of 30% hydrogen peroxide (18 mL). A colour change typically confirmed higher oxidation levels of graphite from brown to yellow. The generated graphite oxide was further purified using 1 M HCl (total of 20 mL) followed by the addition of M.Q. water (using a total of 1 L) using six rounds of centrifugation (Centrifuge 5810 R) at 4000 rpm for 10 min. The supernatant was decanted before the next round of centrifugation until the supernatant became neutral. The final substrates were vacuum dried at 80 °C for 10 h. The whole procedure was carried out 5 times as a reproducible method.

2.3 Synthesis of the CuO-rGO nanomaterial

A composite CuO-rGO material was synthesised according to a method given in Rajapaksha *et al.*, 2019.[40] In short, GO (1.0 g) was mixed with M.Q. water (125.0 mL) and ultra-sonicated for 6 h obtaining a homogenised GO solution at a concentration of 8 mg mL^{-1}. Sodium hydroxide (0.2 M, 50 mL) solution was added into copper(II) sulphate pentahydrate (0.1 M, 50 mL) solution drop-wise at a speed of 10 mL min^{-1} and stirred magnetically at a moderate constant speed for 15 min. The resulting chemical solution mixture was added into the GO

solution drop-wise. Sodium borohydride (0.8 mM, 4 mL) was added drop-wise into the mixture as a reducing agent under moderate constant stirring and the uncovered mixture in the flask was heated at 60 °C for 2 hours. The solution was centrifuged at 4000 rpm for 10 min (Centrifuge 5810 R), decanted where the supernatant was disposed of, and the product then washed with M.Q. water (1 L in total) and centrifuging and washing repeated several times to remove excess reagents. When the supernatant became transparent, the resulting compound was then vacuum dried at 80 °C for 6 h producing CuO doped rGO (CuO-rGO). The whole procedure was carried out in triplicate as a reproducible method.

2.4 Synthesis of the ZnO-rGO nanomaterial

The synthesised GO was hybridised with ZnO following a series of thermal, chemical reactions. In short, GO (1 g) was mixed with M.Q. water (125 mL) and ultra-sonicated for 4 h obtaining a homogenised GO solution at a concentration of 8 mg mL^{-1}. A sodium hydroxide solution (0.2 M, 50 mL) was added into a zinc sulphate heptahydrate (0.1 M, 50 mL) solution and then stirred magnetically at a moderate constant speed for 15 min. The resulting chemical mixture was added into the GO solution. Sodium borohydride (0.8 mM, 4 mL) was added drop-wise into the mixture as a reducing agent under constant moderate stirring in the uncovered flask and the mixture heated at 60 °C for 2 h. The solution was then centrifuged at 4000 rpm for 10 min, decanted where the supernatant was disposed of, and the product then washed with M.Q. water (1 L in total) several times to remove the excess reagents. When the supernatant became transparent, the resulting compound was vacuum dried at 80 °C for 6 h, producing ZnO doped rGO (ZnO-rGO). The whole procedure was carried out in triplicate as a reproducible method.

2.5 Characterisation

2.5.1 Scanning electron microscopy (SEM). The GO nanomaterial (~5 mg) was mixed thoroughly with absolute ethanol, sonicated, and vortexed, and a single drop of the solution (10 μL) was then deposited on a cleaned silicon wafer and air-dried (2 h) inside a fume cabinet. The GO thin film was iridium coated (3 nm) using a sputter coating system (LEICA EM ACE600). The surface morphology of the GO nanomaterial was visualised under an FEI Quanta 200 SEM with an accelerating voltage of 30 kV and a working distance of 10 mm. The protocol was followed similarly for CuO-rGO and ZnO-rGO nanomaterials.

2.5.2 Transmission electron microscopy (TEM). The GO nanomaterial (~5 mg) was mixed thoroughly with absolute ethanol, sonicated and then vortexed; a drop (5 μL) of the solution was taken and dropped onto a thick carbon-coated TEM grid and allowed to air dry for 2 h. The imaging was performed on a TEM (JEOL JEM-2100 FEGTEM) at an accelerating voltage of 200 kV equipped with a Gatan OneView 4k camera. Processing of images was performed using a digital micrograph. A similar TEM protocol was followed for CuO-rGO and ZnO-rGO nanomaterials.

2.5.3 Attenuated total reflectance Fourier transform mid-infrared spectroscopy (ATR-FTIR). The chemical signatures for GO, CuO-rGO and ZnO-rGO materials were analysed with an ATR-FTIR spectrophotometer (Bruker, Alpha II, Germany) operating in the range of 4000–400 cm^{-1} at room temperature in air as the background. OPUS 8.5 Software (Bruker, Germany) was employed to process the spectra identifying the prominent peaks. The spectral resolution was given in wavenumbers (cm^{-1}) and vibrational bands were received at every 2 cm^{-1} for the solid adsorbents.

2.6 Batch adsorption experiments

2.6.1 Textile dyes. A GO (10 mg) adsorbent sample was added into R-6G (10 ppm, 20 mL) and MG (10 ppm, 20 mL) aqueous solutions separately. The R-6G + GO and MG + GO mixtures were shaken at 150 rpm (Bioline incubator shaker 8500) at 25 °C and pH 7 for 6 h until an equilibrium state was reached. The solutions were then filtered using nylon syringe filters (FilterBio) and syringes (5 mL, TERUMO) obtaining adsorbent-free solutions. The solution (500 μL) was then added into a micro UV-cuvette (12.5 × 12.5 × 45 mm, BRAND GMBH + CO KG) and the absorbance of the solution was measured using a UV-visible spectrophotometer (UV-vis CARY3500) at absorption maxima (λ_{max}) at 527 nm and 617 nm wavelengths for R-6G and MG, respectively. The absorbance *vs.* concentration was plotted to provide a concentration calibration for the R-6G and MG dyes (ESI Fig. S1†). The amounts of adsorbed R-6G and MG dyes on the adsorbents were calculated by referring to the calibration plots at their maximum absorption wavelengths as follows:

$$\text{Adsorbed dye concentration} = \frac{C_o - C_e}{W} \times V \quad (1)$$

$$\text{Dye removal efficacy } (\%) = \frac{(C_o - C_e)}{C_o} \times 100 \quad (2)$$

where C_o and C_e (mg L^{-1}) are the liquid-phase concentrations of dye initially and after treatment, respectively. V (L) is the volume of the solution and W (g) is the mass of used adsorbent. The whole protocol was carried out similarly in duplicate trials for GO, CuO-rGO and ZnO-rGO nanomaterials comparing the textile dye removal efficacies of the different adsorbents.

2.6.2 Antibiotics. The GO (10 mg) was added into AMOX (20 ppm, 20 mL) and TC (20 ppm, 20 mL) aqueous solutions separately. The AMOX + GO and TC + GO mixtures were shaken at 150 rpm (Bioline incubator shaker 8500) at 25 °C and pH 7 for 6 h until an equilibrium state was reached. The solutions were then filtered using nylon syringe filters (FilterBio) and syringes (5 mL, TERUMO) to generate adsorbent-free solutions. Antibiotics were analysed according to the UV-visible spectroscopy method developed by Rufino *et al.*, 2010.[41] The filtered AMOX solution (1 mL) was pipetted into a glass vial (10 mL) and mixed with 1% w/v Na$_2$CO$_3$ (70 μL) and 6% w/v chloramine-T trihydrate (250 μL) and kept still for 15 min. The absorbance values were recorded for their maximum absorption wavelengths (λ_{max}) at 385 nm for AMOX and 535 nm for TC, respectively, on a UV-vis spectrophotometer (UV-vis CARY3500). The calibration plots

were prepared using these wavelengths over a series of AMOX and TC antibiotic concentrations (ESI Fig. S1†). The amounts of adsorbed AMOX and TC antibiotics on the adsorbents were calculated by referring to the calibration plots as follows:

$$\text{Adsorbed antibiotic concentration} = \frac{C_o - C_e}{W} \times V \quad (3)$$

$$\text{Antibiotic removal efficacy } (\%) = \frac{C_o - C_e}{W} \times 100 \quad (4)$$

where C_o and C_e (mg L^{-1}) are the liquid-phase concentrations of antibiotic initially and after treatment, respectively. V (L) is the volume of the aqueous solution and W (g) is the mass of used adsorbent. The whole protocol was carried out in duplicate trials similarly for GO, CuO-rGO and ZnO-rGO nanomaterials comparing the antibiotic removal efficacies of the different adsorbents.

The GO, CuO-rGO and ZnO-rGO materials were then analysed for their ability to remove the R-6G and MG dyes and AMOX and TC antibiotics at varied temperature profiles (25 °C, 40 °C, and 60 °C), pH (basic, pH 12; neutral, pH 7; acidic, pH 2), adsorbent dosage (1 mg mL^{-1}, 2 mg mL^{-1}, 3 mg mL^{-1}) and contact time (1 hour time intervals over a 6 h period of time).

2.6.3 Regeneration study. Each adsorbent was regenerated by mixing the used adsorbent with 5% HCl (10 mL) as the desorption agent and this desorption of adsorbed contaminant ions from the GO material will restore the adsorbents for future use.[42] The desorption mixture was sonicated for 30 min and the adsorbent material was then washed with M.Q. water 3 times after removing the supernatant, and dried at 50 °C for 6 h. The regeneration cycles proved an ability to remove the dyes and antibiotics from aqueous solutions as a valid reusable material.

2.6.4 Competitive adsorption study. The competitive behaviour of the R-6G and MG dye molecules when exposed to the GO, CuO-rGO and ZnO-rGO materials was determined by mixing R-6G (10 ppm, 20 mL) and MG (10 ppm, 20 mL) aqueous dye solutions together in a similar experimental setup. Similarly, the competitive behaviour of the AMOX and TC antibiotic molecules was determined by mixing AMOX (20 ppm, 20 mL) and TC (20 ppm, 20 mL) aqueous antibiotic solutions.

2.6.5 Reusing and recycling the adsorbents. The stability and reusability of the GO, CuO-rGO and ZnO-rGO adsorbent materials for removing the dyes and antibiotics were analysed by repeating the adsorption experiment for up to 5 cycles under the optimised temperature, pH, and adsorbent dosage conditions.

The GO, CuO-rGO and ZnO-rGO adsorbents were collected after 5 cycles of adsorption of dyes (R-6G and MG) and antibiotics (AMOX and TC) separately. The adsorbents were dried at 50 °C for 5 h and analysed for their changes in chemical signatures using an ATR-FTIR spectrophotometer (Bruker, Alpha II, Germany) according to the given method in Section 2.5.

2.7 Kinetic study and mathematical modelling

Pseudo-first-order (eqn (5)) and pseudo-second order (eqn (6)) kinetic models were applied to show the mechanism of the

© 2022 The Author(s). Published by the Royal Society of Chemistry

Environ. Sci.: Adv., 2022, **1**, 456–469 | **459**

textile dye and antibiotic adsorption on the GO, CuO-rGO and ZnO-rGO adsorbents.

$$\log(q_e - q_t) = \log(q_e) - \frac{K_1}{2.303}t \quad (5)$$

$$\frac{1}{q_t} = \frac{1}{K_2(q_e)^2} + \frac{t}{q_e} \quad (6)$$

where K_1 is the first order rate constant of adsorption (min^{-1}), t is time, and K_2 is the pseudo-second-order rate constant in g mg^{-1} min^{-1}.

The Langmuir isotherm models were used to understand the distribution of dye and antibiotic molecules on the surface of GO, CuO-rGO and ZnO-rGO solid materials and the aqueous phase at equilibrium state. The following equation was used for the Langmuir isotherm modelling.

$$q_e = \frac{q_{max}K_1 C_e}{1 + K_1 C_e} \quad (7)$$

The Langmuir adsorption parameters were then linearised into the following equation.

$$\frac{C_e}{q_e} = \frac{C_e}{q_{max}} + \frac{1}{q_{max}K_1} \quad (8)$$

where q_{max} corresponds to the maximum amount of dye/antibiotic per unit weigh of adsorbent (mg mL^{-1}) and K_1 represents the Langmuir adsorption constant (L mg^{-1}).

2.8 Thermodynamic analysis

The Gibbs free energy (ΔG) of adsorption of dyes and antibiotics was calculated using the following equation.

$$\Delta G = RT \ln K_1 \quad (9)$$

where K_1 is the Langmuir adsorption constant (L mg^{-1}), T is the temperature (K) and R is the universal gas constant (8.314 J mol^{-1} K^{-1}).

2.9 Statistical and mathematical analysis

All statistical and mathematical analyses including the mean, standard deviation, regression coefficients regarding the kinetics, mathematical modelling and thermodynamic analyses were performed using Origin 8.5 software.

3 Results and discussion

3.1 Characterisation

The scanning electron (Fig. 2a) and TE micrographs (Fig. 2b) show clear differences between each material: GO (Fig. 2(i and iv)) and before and after the addition of CuO (Fig. 2(ii and v)) and ZnO (Fig. 2(iii and vi)) metal nanoparticles. The GO showed a wrinkled multi-layered and folded nanostructure morphology which provides ample sites for diffusion of the dye and antibiotic molecules facilitating their adsorption. The CuO and ZnO nanofunctionalised GO materials were morphologically different to the GO, showing crystalline amorphous structures
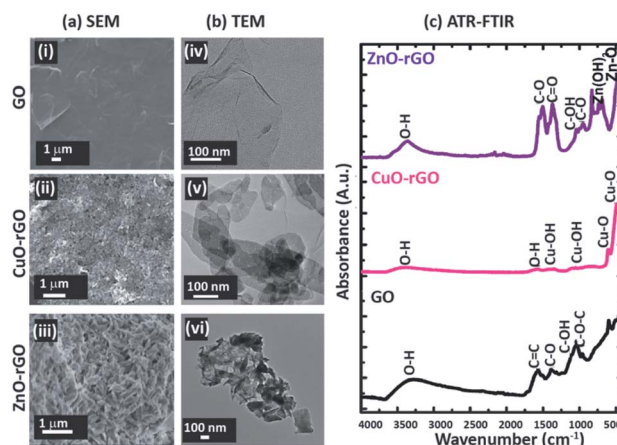

Fig. 2 The surface morphological analyses of (a) SEM: (i) GO, (ii) CuO-rGO, (iii) ZnO-rGO; (b) TEM: (i) GO, (ii) CuO-rGO, (iii) ZnO-rGO; and (c) ATR-FTIR showing the chemical signatures on GO, CuO-rGO and ZnO-rGO.

(Fig. 2a(ii and iii)). The CuO and ZnO particles were distributed unevenly on the rGO. The GO material exhibited a typical 'flaky' characteristic feature, while CuO-rGO and ZnO-rGO showed a densely packed and random distribution of CuO and ZnO materials, respectively. The ZnO deposition on rGO made the ZnO-"nanoflowers" form sharp edges (Fig. 2(iii)). The ATR-FTIR spectrum of the GO showed strong bands of absorbance at 3323 cm^{-1}, 1575 cm^{-1}, 1387 cm^{-1}, 1119 cm^{-1} and 1065 cm^{-1} representing O–H, C=C, C–O, C–OH and C–O–C vibrations respectively (Fig. 2c).[40] The functional groups on the GO were further identified using the XPS at C 1s spectra (ESI Fig. S2†). In the CuO-rGO, strong peaks were observed at 502 cm^{-1} and 612 cm^{-1} that are associated with Cu–O vibrations of CuO.[43,44] The peaks at 1127 cm^{-1} and 1378 cm^{-1} for the CuO-rGO are attributed to Cu–O and Cu–OH vibrations.[43] The hydroxyl groups of CuO-rGO were further confirmed by the O–H stretching at 1616 cm^{-1}.[44] The ZnO-rGO shows strong chemical peaks at 473 cm^{-1} and 671 cm^{-1} due to the Zn–O and Zn–OH vibrations respectively.[45] The additional chemical signals for ZnO-rGO at 3387 cm^{-1}, 1520 cm^{-1}, 1380 cm^{-1}, 1057 cm^{-1} and 966 cm^{-1} represent O–H, C=O, C–O, C–OH and C–O vibrations respectively.[45,46]

3.2 Batch adsorption experiments

3.2.1 Effect of pH. The pH in an aqueous solution plays an important role in the adsorption of dyes (Fig. 3A) and antibiotics (Fig. 4A) on the adsorbents. This role is because the pH of the aqueous solution alters the charge of the functional groups attached to the adsorbents.[25,47] The GO and rGO consist of negatively charged functional groups (Fig. 2c) on their surface.[48,49] The charge of the surface of the GO and rGO adsorbents is neutralised more by the acidic aqueous solutions.[50] The pH of the aqueous solution affects the electrostatic attraction between the contaminants and adsorbents.[25] Therefore, the adsorption of cations can undergo a competitive effect with H^+ ions in aqueous solutions. As a result, the adsorption of
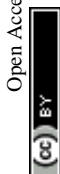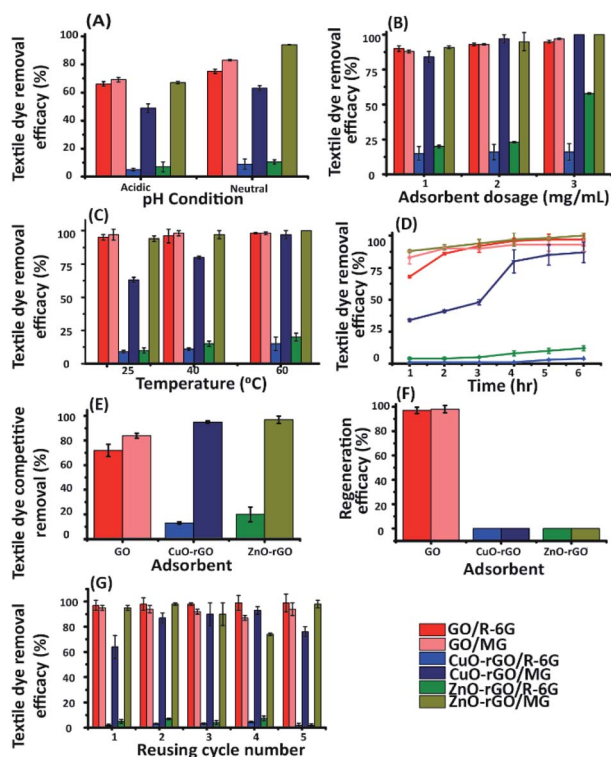
Fig. 3 Batch adsorption analysis of R-6G and MG using GO, CuO-rGO and ZnO-rGO nanocomposite materials analysing the effect of (A) pH of the aqueous solution (acidic-pH 2, neutral-pH 7); (B) adsorbent dosage (1 mg mL^{-1}, 2 mg mL^{-1}, 3 mg mL^{-1}); (C) temperature (25 °C, 40 °C, 60 °C); (D) contact time with 1 h time intervals until reaching the equilibrium state at 4 h. (E) Competitive adsorption between the R-6G and MG dyes on the adsorbents, showing that the MG dye preferentially adsorbed in such a system when compared to R-6G. (F) Regeneration experiments of the adsorbents showing GO with 98% maximum regeneration capacity. (G) The recycling of GO, CuO-rGO and ZnO-rGO adsorbents provided 5 effective cycles, showing the maximum recycling efficacy of GO for removing the R-6G and MG dyes from aqueous solutions.
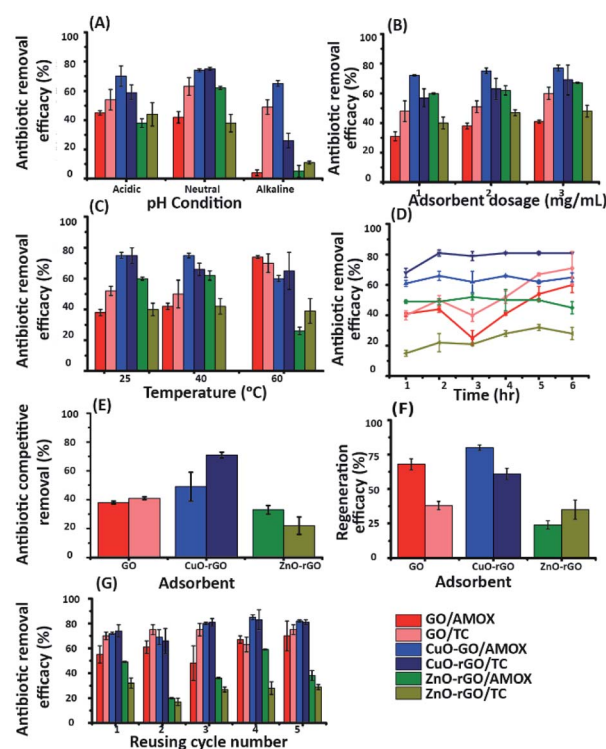

Fig. 4 Batch adsorption analysis of AMOX and TC on GO, CuO-rGO and ZnO-rGO nanocomposites analysing the effect of (A) pH of the aqueous solution (acidic-pH 2, neutral-pH 7, basic-pH 12); (B) adsorbent dosage (1 mg mL^{-1}, 2 mg mL^{-1}, 3 mg mL^{-1}); (C) temperature (25 °C, 40 °C, 60 °C); (D) contact time with 1 h time intervals within 6 h. (E) Competitive adsorption patterns of AMOX and TC antibiotics on the adsorbents. (F) Regeneration of adsorbents showing AMOX adsorbed CuO-rGO with 80% maximum regeneration capacity. (G) The recycling of GO, CuO-rGO and ZnO-rGO adsorbents up to 5 recycling rounds, showing the maximum recycling efficacy of CuO-rGO for removing both AMOX and TC antibiotics from aqueous solutions.

contaminant cations on the GO materials is limited under acidic conditions.[4] The R-6G and MG dyes are cationic dyes[51] (ESI Fig. S3†) and therefore are better adsorbed under neutral and basic pH conditions, because the negatively charged adsorption sites on the GO, CuO-rGO and ZnO-rGO adsorbents are not typically affected by OH$^-$ ions. The MG reacted with NaOH and this caused the solution to decolourise instantly. As recorded in previous studies, the reason for this decolourisation is the changes in the planar ring system of the MG molecule that is attacked by the OH$^-$ ions from NaOH[52] (ESI Fig. S4†) and therefore, neutral aqueous solutions were used in batch experiments. This is an important optimisation experiment to demonstrate the material's ability. Usually surface waters including rivers, streams and lakes have a pH of 6–8,[53] and the standard pH for industrial wastewater discharges remains at pH 6–9, and thus in general these pH values are within the range used to remove the dyes in the current study. In contrast to the textile dyes, the AMOX and TC antibiotic molecules (ESI Fig. S3†) are anionic in aqueous media,[54,55] and therefore these

molecules are efficiently adsorbed under neutral pH conditions, where the positively charged metal ions on CuO-rGO and ZnO-rGO are not affected by the neutral pH aqueous solution. The ionisation and hydration of antibiotic molecules under neutral pH conditions are lower, facilitating the adsorption process *via* hydrogen bonding and π–π stacking.[56] The antibiotic adsorption efficacies using CuO-rGO and ZnO-rGO adsorbents decreased with increasing pH, because the positive charge of the nanocomposites was neutralised by the OH$^-$ ions from the aqueous solutions. In brief, the GO material was the most suitable adsorbent for removing both R-6G and MG dye molecules under neutral and alkaline pH conditions. The CuO-rGO was the most effective adsorbent for removing both antibiotics under neutral pH conditions.

3.2.2 Effect of adsorbent dosage. Adsorbent dosages (1, 2, and 3 mg mL^{-1}) of GO, CuO-rGO and ZnO-rGO were analysed against the dyes (10 ppm, Fig. 3B) and antibiotics (20 ppm, Fig. 4B). For R-6G removal, the GO material was 90% effective and 15–16% was removed using the CuO-rGO material in all dosages. This may be due to the overlapping or aggregation of adsorption sites during increasing the adsorbent dosage for the

© 2022 The Author(s). Published by the Royal Society of Chemistry

Environ. Sci.: Adv., 2022, **1**, 456–469 | **461**

contaminant dyes.[4] The MG removal was gradually increased with increased adsorbent dosages and ~100% MG removal was observed at 3 mg mL^{-1} using GO, CuO-rGO and ZnO-rGO, which is due to the increased adsorption sites provided. The adsorption of both AMOX and TC antibiotics on GO, CuO-rGO and ZnO-rGO was also gradually increased by the increased adsorbent dosages. The best antibiotic removal was recorded (80%) by CuO-rGO at 3 mg mL^{-1} dosage.

3.2.3 Effect of temperature.
The effect of temperature on adsorption was studied at 25 °C, 40 °C and 60 °C; these temperatures are practice standards in wastewater purification. The dye removal was gradually increased with increasing temperature. The optimum temperature for removing both the dye molecules was 60 °C, demonstrating that the higher temperature values affect the kinetic energy of the dye molecules to be adsorbed.[57] The GO recorded the highest removal of R-6G (95%) and MG (100%) at 60 °C. The removal of dyes and the process of adsorption was noticeably different for pharmaceutical depollution, where AMOX and TC antibiotic removal using the CuO-rGO and ZnO-rGO remained highest at both 25 °C and 40 °C demonstrating a 75% adsorption efficacy. The antibiotic removal was decreased when increasing temperature to 60 °C. The optimum temperature for the adsorption of TC on rGO in previous studies was 45 °C (ref. 58) which corroborates with our findings in this work. However, the adsorption efficacy for the removal of AMOX and TC using the GO adsorbent increased at 60 °C. This increase in temperature may be due to the different molecular activities influenced by antibiotics at the solid–solution interface. The stochastic kinetics of the antibiotic molecules at the solid–solution interface increased at 45 °C exposed to rGO and at 60 °C exposed to GO. The effect of temperature for the dye and pharmaceutical adsorption is further elaborated in the kinetic study and mathematical modelling (Section 3.3) and thermodynamic analyses (Section 3.4).

3.2.4 Effect of contact time.
The adsorption of the dyes on GO, CuO-rGO and ZnO-rGO rapidly increased during 0–30 min and reached equilibrium at 4 h (240 min). There was no noticeable dye adsorption rate change after 240 min. Similar equilibrium states (240 min) were observed for MG adsorption which is commensurate with previous work using a modified GO material (Fe$_3$O$_4$/Pt/GO) adsorbent and MG dye.[4] The reason is the binding sites on the adsorbents were vacant for the contaminants at the beginning and these binding sites were gradually occupied and saturated by contaminants within 240 min.[59] After the equilibrium state, the adsorbent sites were becoming unavailable and repulsive forces existed between the adsorbent and contaminants.[60] The removal of AMOX and TC antibiotics using the CuO-rGO and ZnO-rGO also behaved similarly, achieving a state of equilibrium at 240 min. The CuO-rGO recorded maximum antibiotic removal of 80% and 60% for removing AMOX and TC respectively during the 240 min period.

3.2.5 The reuse and recycling of adsorbents.
Being able to reuse the adsorbent materials is an attractive property and important factor for efficiency and cost-effectiveness in the wastewater treatment process.[61] Five consecutive recycle runs were carried out for each adsorbent for the dye (Fig. 3G) and the antibiotic/pharmaceutical (Fig. 4G) molecules. The GO

adsorbent was regenerated after the first adsorption run of dyes (Fig. 3F) using hydrochloric acid, because desorption of an adsorbent can be achieved by proton exchange using an acid.[42] Upon acidifying the GO material high dye removal values (97% for R-6G and 98% for MG) were achieved. This was shown to be an average of 9.8 mg mL^{-1} when quantified using UV-vis spectroscopy. These values indicate that the material is reusable which could show potential as an environmentally friendly multi-use water depollution material. The CuO-rGO and ZnO-rGO materials were poorly regenerated for the dye adsorption (Fig. 3F), which is due to the loss of available adsorption sites on the adsorbents after the desorption treatment. This occurs when all the initial adsorption sites have not been significantly removed.[60] The GO, CuO-rGO and ZnO-rGO were regenerated and then tested in cycles against the antibiotics removal (Fig. 4F) with 68%, 80%, and 20% for AMOX and 38%, 61%, and 35% for TC. The CuO-rGO performed well when removing antibiotics and with a number of regeneration cycles. The CuO-rGO material maintained an average of 80% adsorption capacity of antibiotics from the system, indicating that the stability and reusability of the antibiotic from the contaminated system would hold firm.

The ZnO-rGO regeneration efficiency was lowest under acidic conditions, and this may be due to the presence of H$^+$ ions resulting in an interaction with the strongly bound ZnO on the rGO.[4] Therefore, the authors suggest that the ZnO-rGO is stable under acidic conditions. Further, the dye and antibiotic contaminants were efficiently removed using neutral experimental conditions for the regeneration experiments. This is because the H$^+$ ions from acids and OH$^-$ from alkaline solutions undergo competitive behaviours with the cationic and anionic contaminants, towards the rates of adsorption. Therefore, the nanomaterials were found to be most effective when they were pre-neutralised.

3.2.6 Analysing the competitive removal behaviours of the contaminant molecules.
The R-6G and MG dyes (Fig. 3E) and AMOX and TC antibiotics (Fig. 4E) were mixed together separately, in order to analyse the effect of competitive behaviour of each molecule towards adsorption on GO, CuO-rGO and ZnO-rGO (Section 2.6) materials. MG was readily removed more than the R-6G from the GO, CuO-rGO and ZnO-rGO. The reason is that MG showed 8% photodegradation from 10 ppm concentration without using an adsorbent after 6 hours under the same experimental conditions as in Section 3.2 (ESI Fig. S5†). The photodegradation activity of MG has been recorded similarly in previous studies.[62,63] This photocatalytic degradation was not shown from R-6G dye and R-6G remained stable in its concentration throughout the time. This clarifies that MG removal relies on both photo-degradation and adsorption and R-6G relies completely on adsorption. In a mixture of antibiotics, TC was attracted more than AMOX onto the GO and CuO-rGO. This might be due to the more aromatic rings of TC molecules compared to AMOX, which are responsible for making π–π interactions with the adsorbent (ESI Fig. S3†).[54,64]

The dye and antibiotic removal efficacy using GO, CuO-rGO and ZnO-rGO materials under the optimised conditions were compared to the rGO material (ESI Fig. S6†). The rGO was an excellent adsorbent for removing cationic dyes compared to CuO-

rGO and ZnO-rGO. We observe a reduction in the density of adsorption sites of the rGO when doped with the metal nanoparticles. Further, ZnO and CuO in the nanocomposites limit the attraction of cationic contaminant molecules in the rGO, due to cationic–cationic repulsion. Meanwhile, GO demonstrated excellent adsorbent properties (95% and 97%) for R-6G and MG dyes. The anionic compounds (antibiotics) and their removal using rGO proved to be less than GO, CuO-rGO, and ZnO-rGO, being 45% and 39% for AMOX and TC respectively. This result suggests that CuO and ZnO are involved in the adsorption of anionic contaminant molecules on the rGO due to electrostatic interactions. This is discussed in detail under Section 3.5.

3.3 Kinetic study and mathematical modelling

The adsorption of dyes and antibiotics on GO, CuO-rGO and ZnO-rGO fitted to the pseudo-second order kinetic model
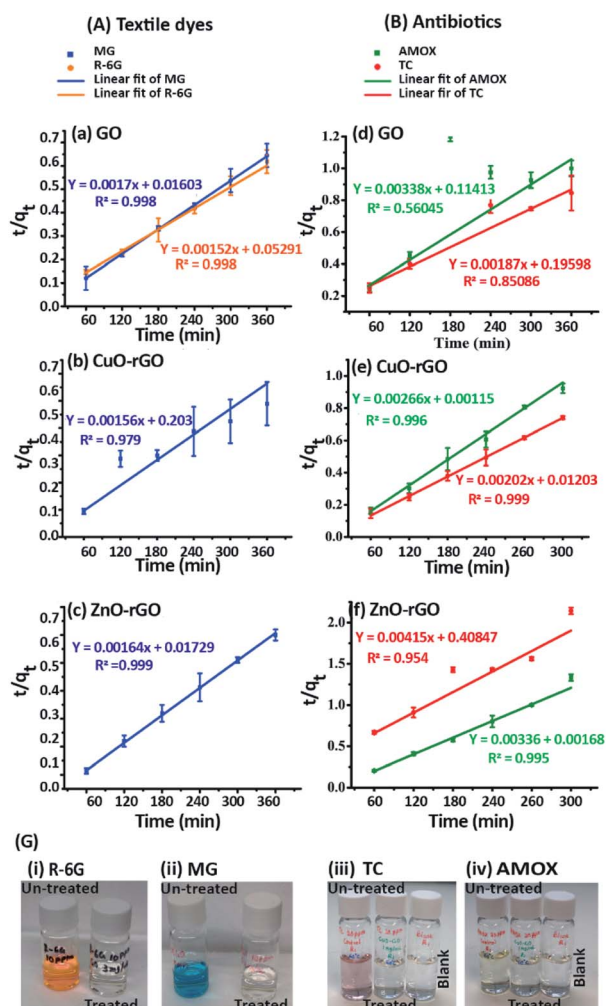
(Fig. 5) showing an accurate linear fitting with high R^2 coefficient values at 333 K. The adsorption kinetics were not included for R-6G dye molecules on CuO-rGO and ZnO-rGO adsorbents (Fig. 5), due to the negligible adsorption capacities of 1–4% and 4–12% respectively.

The calculations demonstrate that the adsorption of dyes and antibiotics on the adsorbents has occurred according to the pseudo-second order kinetic model suggesting that both the adsorbents and contaminants have engaged in a rate of reaction and therefore contaminants are adsorbed *via* chemisorption processes.[65] The calculated equilibrium sorption (q_e) capacities for the dye antibiotic molecules are given in Table 1.

Langmuir isotherm modelling was carried out assuming that the monolayer coverage of the dye and antibiotic molecules on the GO, CuO-rGO and ZnO-rGO adsorbent surfaces was homogeneous. The calculations were carried out assuming that there were identical and energetically equivalent adsorption sites without the interaction between the contaminant molecules.[25,66] The experimental data of the adsorption of dye and antibiotic molecules on GO, CuO-rGO and ZnO-rGO adsorbents were well fitted on the Langmuir isotherm model showing the best fit of R^2 values ($R^2 > 0.9$). The q_{max} and the K_L values were calculated using the slope and the intercept of the linearised plots of the Langmuir isotherm models (Fig. 6). The q_{max} values of the adsorbents are given in Table 1.
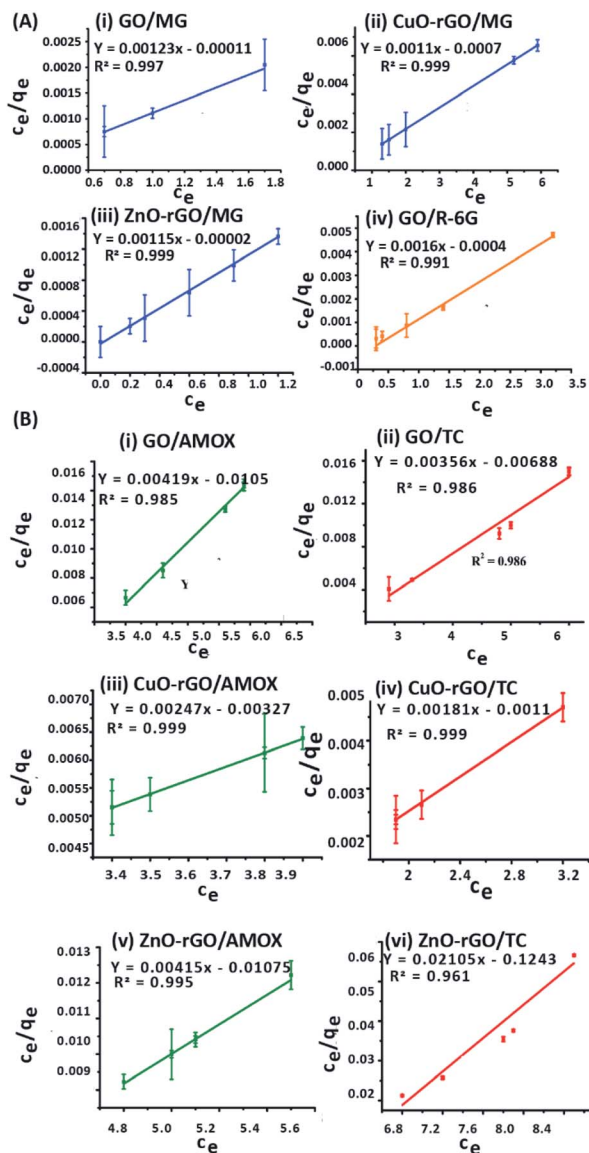
The MG adsorption was highly favourable towards all three GO, CuO-rGO and ZnO-rGO recording the highest q_{max} values, while R-6G adsorption was favoured by only GO. CuO-rGO recorded the highest q_{max} values for the adsorption of both AMOX and TC antibiotics, and appears to be the most suitable adsorbent for the adsorption of antibiotics. The q_{max} values for removing dyes and antibiotics from the GO, CuO-rGO and ZnO-rGO adsorbents in the current study were significantly higher than the previously recorded studies (ESI Tables 1 and 2†), showing their suitability towards the adsorption processes of contaminant molecules in polluted water systems.

3.4 Thermodynamic analysis

Thermodynamic analysis was carried out at 298 K, 313 K and 333 K temperatures for the adsorption of dyes and antibiotics

Fig. 5 Pseudo-second order kinetics plots for (A) textile dye adsorption of (a) R-6G and MG adsorption on GO, (b) MG adsorption on CuO-rGO, (c) MG adsorption on ZnO-rGO and (B) antibiotic adsorption of (d) AMOX and TC on GO, (e) AMOX and TC on CuO-rGO and (f) AMOX and TC on ZnO-rGO, (G) visual colour representations before and after treatments of (i) R-6G and (ii) MG dyes and (iii) TC and (iv) AMOX antibiotics.

Table 1 Equilibrium sorption capacities (q_e) and maximum adsorption capacities (q_{max}) for the dye and antibiotic molecules

Contaminant/adsorbent	q_e (mg g^{-1})	q_{max} (mg g^{-1})
R-6G/GO	658	625
MG/GO	575	813
MG/CuO-rGO	641	909
MG/ZnO-rGO	610	870
AMOX/GO	296	239
AMOX/CuO-rGO	376	404
AMOX/ZnO-rGO	298	241
TC/GO	535	281
TC/CuO-rGO	495	552
TC/ZnO-rGO	241	48

© 2022 The Author(s). Published by the Royal Society of Chemistry

Environ. Sci.: Adv., 2022, **1**, 456–469 | **463**

Fig. 6 The equilibrium Langmuir isotherm model fitting for the adsorption of (A) textile dyes: (i) MG on GO, (ii) MG on CuO-rGO, (iii) MG on ZnO-rGO and (iv) R-6G on GO, and (B) antibiotics: (i) AMOX on GO, (ii) TC on GO, (iii) AMOX on CuO-rGO, (iv) TC on CuO-rGO, (v) AMOX on ZnO-rGO and (vi) TC on ZnO-rGO. The Langmuir isotherm model was used for understanding the distribution of the dyes and antibiotic contaminant molecules in the liquid and solid phases of the aqueous solution characterising the state of equilibrium.

on GO, CuO-rGO and ZnO-rGO adsorbents analysing the Gibbs free energy change ($\Delta G°$) (eqn (9)), enthalpy change ($\Delta H°$) and entropy change ($\Delta S°$) from the derived equations as follows;

$$\Delta G° = -RT \ln K_c$$

$$K_c = \frac{C_o}{C_e}$$

$$\Delta G = \Delta H - T\Delta S$$

$$\ln K_c = \frac{\Delta S°}{R} - \frac{\Delta H°}{RT}$$

where K_c = thermodynamic equilibrium constant, R = 8.314 J mol^{-1} K^{-1} (gas constant), T = temperature (K), C_o = initial contaminant concentration (mg mL^{-1}) and C_e = equilibrium contaminant concentration (mg L^{-1}). The $\Delta S°$ and $\Delta H°$ were determined from the intercept and slope of the linearised graph of $\ln K_c$ *versus* $1/T$ (ESI Fig. S7†).

The negative $\Delta G°$ values suggested that the adsorption of R-6G and MG dyes (Table 2) and AMOX and TC antibiotics (Table 3) on each of GO, CuO-rGO and ZnO-rGO adsorbents at 298 K,

Table 2 Thermodynamic parameters for the adsorption of textile dyes

Dye/adsorbent	T (K)	$\Delta G°$ (kJ mol^{-1})	$\Delta H°$ (kJ mol^{-1} K^{-1})	$\Delta S°$ (J mol^{-1} K^{-1})
R-6G/GO	298	−7.42	21.86	97.68
	313	−8.37		
	333	−10.83		
R-6G/CuO-rGO	298	−0.23	1.62	6.15
	313	−0.33		
	333	−0.44		
R-6G/ZnO-rGO	298	−0.26	2.70	10.14
	313	−0.42		
	333	−0.61		
MG/GO	298	−8.68	9.25	60.85
	313	−10.18		
	333	−10.83		
MG/CuO-rGO	298	−2.46	59.95	207.85
	313	−4.18		
	333	−9.70		
MG/ZnO-rGO	298	−6.97	42.40	165.28
	313	−9.12		
	333	−12.74		

Table 3 Thermodynamic parameters for the adsorption of antibiotics

Antibiotic/adsorbent	T (K)	$\Delta G°$ (kJ mol^{-1})	$\Delta H°$ (kJ mol^{-1} K^{-1})	$\Delta S°$ (J mol^{-1} K^{-1})
AMOX/GO	298	−1.18	20.9	73.24
	313	−1.41		
	333	−3.72		
AMOX/CuO-rGO	298	−3.43	−11.37	−25.93
	313	−3.60		
	333	−2.53		
AMOX/ZnO-rGO	298	−2.27	−14.95	−41.57
	313	−2.51		
	333	−0.83		
TC/GO	298	−1.81	11.43	43.64
	313	−1.80		
	333	−3.33		
TC/CuO-rGO	298	−3.43	−7.71	−14.79
	313	−2.80		
	333	−2.90		
TC/ZnO-rGO	298	−1.26	−0.44	−2.86
	313	−1.41		
	333	−1.36		

313 K and 333 K temperatures occurred as spontaneous processes with positive $\Delta H°$, indicating that these contaminant molecules are adsorbed as endothermic processes.[25] The AMOX and TC adsorption on GO was an endothermic process due to the positive $\Delta H°$ values and the negative $\Delta H°$ values indicated

that the AMOX and TC adsorption on CuO-rGO and ZnO-rGO was an exothermic process.[67,68]

During the adsorption processes of dyes, the negative $\Delta G°$ values increased with increasing the temperatures of all three adsorbents, suggesting that the process of adsorption of dyes
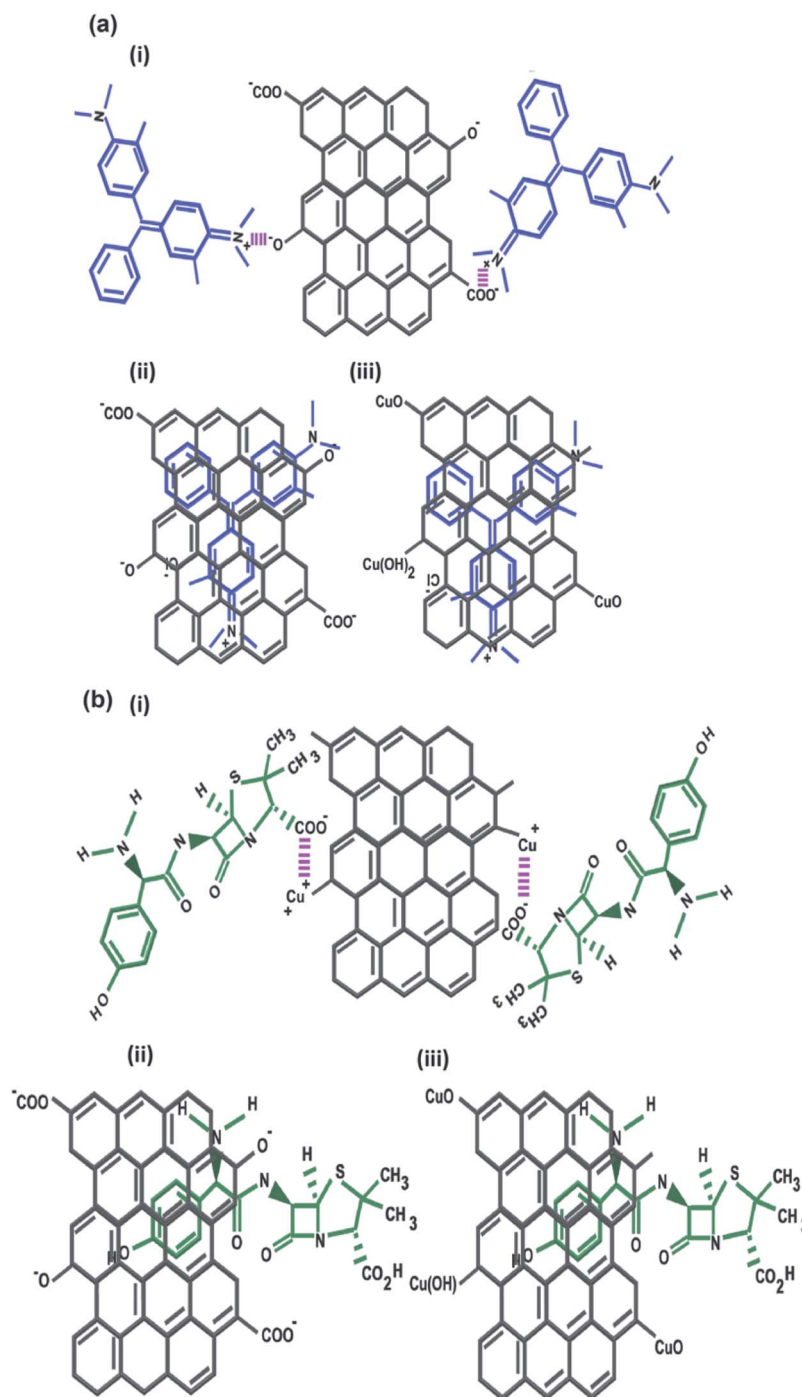

Fig. 7 The plausible adsorption pathways of (a) the representative cationic dye: MG cation on (i) GO *via* electrostatic bonds towards negatively charged functional groups in aqueous media, (ii) GO *via* π–π interactions between aromatic rings of MG and GO and (iii) CuO-rGO *via* π–π interactions between aromatic rings of MG and rGO; (b) representative anionic antibiotic: AMOX anion on (i) CuO-rGO *via* electrostatic interactions towards positively charged metal ion groups on rGO in aqueous media, (ii) GO *via* π–π interactions between aromatic rings of AMOX and GO and (iii) CuO-rGO *via* π–π interactions between aromatic rings of AMOX and rGO.

was more favourable at high temperatures. During the adsorption of antibiotics, the negative $\Delta G°$ value increased with the temperature only for the adsorption of GO, and thus AMOX and TC adsorption on GO was favoured at high temperature. This was proven experimentally above (Section 3.2.3) analysing the effect of temperature on the adsorption behaviour. In contrast to the adsorption of dyes, the highest negative $\Delta G°$ was recorded at 40 °C on adsorption processes of AMOX and TC on CuO-rGO and ZnO-rGO materials. The positive $\Delta S°$ further suggested that the randomness of the molecules at the solid–solution interface

increased during the adsorption on GO, CuO-rGO and ZnO-rGO adsorbent materials.[4,69]

3.5 Plausible adsorption mechanisms

The contribution of the nanoparticles (CuO and ZnO) when incorporated into CuO-rGO and ZnO-rGO as composite materials generated preferential adsorption of anionic or cationic chemical pollutants. These CuO-rGO and ZnO-rGO nanocomposites were shown to be ineffective in the removal of
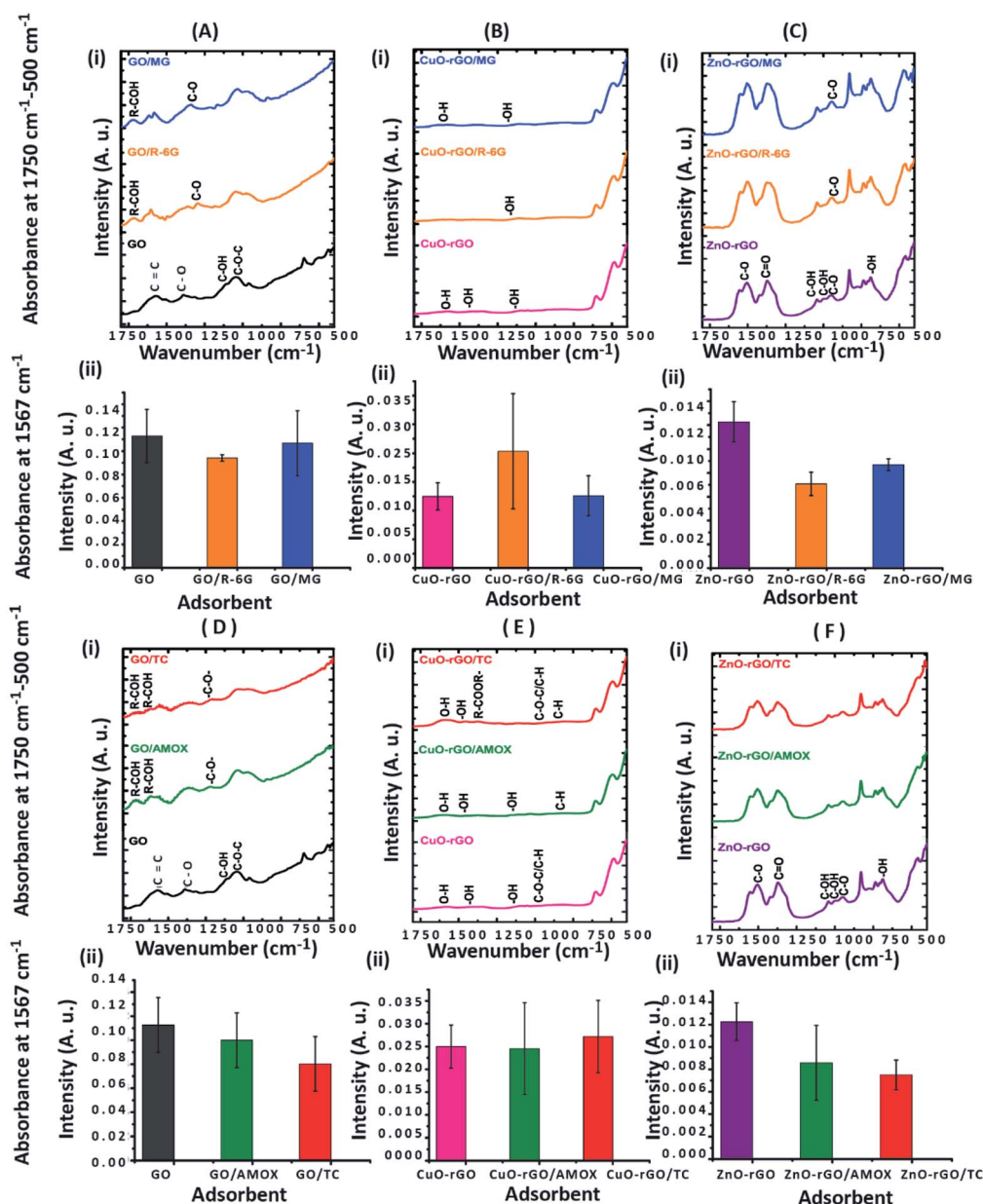

Fig. 8   The analysis of changes of chemical signatures after R-6G and MG dye adsorption on GO (A), CuO-rGO (B) and ZnO-rGO (C) and AMOX and TC antibiotic adsorption on GO (D), CuO-rGO (E) and ZnO-rGO (F) compared to the control adsorbent using an ATR-FTIR spectroscopy method in the range of 1750 to 500 cm^{-1}. The column chart showing the intensity of absorbance at 1567 cm^{-1} owing to C=C vibrations of (A)(ii) GO, (B)(ii) CuO-rGO, and (C)(ii) ZnO-rGO after R-6G and MG adsorption compared to the control adsorbent. The column chart showing the intensity ratio at 1567 cm^{-1} owing to C=C vibrations of (D)(ii) GO, (E)(ii) CuO-rGO, and (F)(ii) ZnO-rGO after AMOX and TC adsorption compared to the control adsorbents.

cationic chemicals for R-6G and MG when compared to the GO material. Additionally, when conducting regeneration experiments for cationic pollutant experiments using the CuO-rGO and ZnO-rGO nanocomposite materials, these did not show significance when examining the adsorption of cationic contaminants. There are several reasons for this result. The first is that incorporating nanoparticles into the rGO nanocomposite reduces the pore density of the material, resulting in varied performances for the materials investigated. However, this would also be true for anionic pollutants, therefore the pore density hypothesis is null. It is the chemical interactions which are at large here, where we observe that for cations, the nanocomposite materials are electrostatically repelling such types of pollutants. The charge of the material is important in this regard, and in Yang et al., 2019,[70] Gupta et al., 2017 (ref. 25) and Liu et al., 2012 (ref. 26) studies have been detailed. Metal oxide doped rGO has a high surface area, and as such does not possess as high a negative charge and is found to be excellent as an adsorbent for anionic molecules. This has been shown in our experiments, where for anionic chemical depollution, the nanocomposite CuO-rGO removed 77% and 69%, and ZnO-rGO removed 67% and 48% of AMOX and TC compared to the GO. The regeneration results for the materials CuO-rGO and ZnO-rGO also showed high regeneration effectiveness and they continued to perform in the removal of anionic contaminants. This is also discussed in Ramesha et al., 2011.[71] There are several adsorption mechanisms of adsorbents such as size-exclusion, electrostatic interactions, hydrophilic interactions, hydrophobic interactions, chemical and hydrogen bond interactions, π–π interactions, competitive ion exchange, pore filling mechanisms and competitive ion exchange.[29] These attractions between the dye and antibiotic contaminants and adsorbents are due to electrostatic interactions (Fig. 7a) and π–π interactions (Fig. 7b).[72,73]

The chemical functional groups on GO adsorbents provide excellent adsorbent sites for water depollution and as we show for certain known wastewater contaminants.[33] The disappearance, appearance, and shifting of chemical signatures in the batch adsorption experiments for dyes and antibiotics on GO reveal that the contaminants have affinity for GO.[74] The plausible adsorption mechanism is that cationic dyes are mainly adsorbed on GO, towards their negatively charged functional groups via electrostatic attractions (Fig. 7a(i)), where maximum adsorption of cationic dyes is recorded on negative functional group rich GO. Further, the adsorption of cationic dyes is possible for both GO and rGO via π–π interactions, where the rGO (CuO-rGO and ZnO-rGO) recorded the minimal dye adsorption. The anionic antibiotic molecule adsorption was maximum towards the CuO-rGO, and the plausible mechanism of adsorption is electrostatic interactions towards positively charged metal ions on rGO (Fig. 7b(i)). The π–π interactions of anionic antibiotics on rGO and GO are plausible (Fig. 7b(ii and iii)), where minimal antibiotic adsorption occurred on GO.

The GO nanomaterial is rich with negatively charged hydroxyl, carboxyl, and carbonyl functional groups (Fig. 2c). The MG and R-6G molecules are cationic in aqueous systems, and are therefore attracted towards negatively charged hydroxyl, carbonyl and carboxylic functional sites via electrostatic interactions (Fig. 7).[75,76] The major changes of the chemical functionalities on GO after adsorption of dyes and antibiotics were observed in the wavenumber range of 1750 to 500 cm^{-1} in the ATR-FTIR spectra. The vibrations at 1387 cm^{-1} and 1119 cm^{-1} on GO attributed to the C–O and C–OH groups respectively were diminished and new peaks appeared at 1738 cm^{-1} and 1588–1594 cm^{-1} owing to C=O and C=C respectively after adsorption of dyes (Fig. 8A(i)) and antibiotics (Fig. 8D(i)) on GO. After adsorption of antibiotics on GO, the peaks at 1575 cm^{-1} and 1065 cm^{-1} owing to C=C and C–O–C respectively were slightly diminished, and chemical signatures at 1400 cm^{-1} and 1242 cm^{-1} were prominent/appeared owing to C–H and C–H$_3$ vibrations respectively.[77] Significant differences were not observed in the ATR-FTIR spectra after adsorption of dyes and antibiotics on CuO-rGO and ZnO-rGO and this might have occurred due to the overlapping of the IR measurement peaks. However absorbance at 1567 cm^{-1} of ATR-FTIR spectra owing to the C=C bonding recorded significant changes on GO after adsorption of both dyes and antibiotics on CuO-rGO (Fig. 8B and E) and ZnO-rGO (Fig. 8C and F) indicating that these changes have occurred as a result of adsorption of dyes and antibiotics.

4 Conclusions

Unmodified GO and nanofunctionalised CuO-rGO and ZnO-rGO were synthesised using a pre-published modified Hummers method with additional thermal chemical reactions to functionalise the nanocomposites. These carbon nanomaterials were evaluated for their adsorption behaviours of textile dyes R-6G and MG, and antibiotics AMOX and TC. The kinetic experiments and mathematical modelling proved that the adsorption processes fitted well into the Langmuir isotherm model and with pseudo-second order kinetic parameters revealing that the adsorption occurred via a series of chemisorption principles. The thermodynamic analysis indicated that all the adsorption processes were spontaneous. The R-6G, MG, AMOX and TC adsorption on the GO was an endothermic process, while R-6G and MG adsorption on CuO-rGO and ZnO-rGO was also an endothermic process. AMOX and TC adsorption on CuO-rGO and ZnO-rGO occurred as an exothermic process. The plausible adsorption pathways are electrostatic attraction and π–π interactions between the contaminants and adsorbents. In summary, the GO material was an efficient adsorbent for the adsorption of cationic textile dyes, and the nanofunctionalised CuO-rGO and ZnO-rGO composite-materials were suitable for the adsorption of anionic antibiotic molecules. GO showed the highest adsorption capacity of 625 mg g^{-1} and 813 mg g^{-1} for removing R-6G and MG dyes respectively. CuO-rGO recorded the highest adsorption of antibiotics with 405 mg g^{-1} and 552 mg g^{-1} for removing AMOX and TC, respectively. The study concludes that GO, CuO-rGO and ZnO-rGO materials are promising adsorbent materials towards wastewater depollution processes.

© 2022 The Author(s). Published by the Royal Society of Chemistry

Environ. Sci.: Adv., 2022, **1**, 456–469 | **467**

Conflicts of interest

There are no conflicts to declare.

Acknowledgements

References

1 B. Lellis, C. Z. Fávaro-Polonio, J. A. Pamphile and J. C. Polonio, *Biotechnol. Res. Int.*, 2019, **3**, 275–290.

2 S. A. Kraemer, A. Ramachandran and G. G. Perron, *Microorganisms*, 2019, **7**, 180.

3 T. aus der Beek, F. A. Weber, A. Bergmann, S. Hickmann, I. Ebert, A. Hein and A. Küster, *Environ. Toxicol. Chem.*, 2016, **35**, 823–835.

4 M. Gao, Z. Wang, C. Yang, J. Ning, Z. Zhou and G. Li, *Colloids Surf., A*, 2019, **566**, 48–57.

5 E. R. Nestmann, G. R. Douglas, T. I. Matula, C. E. Grant and D. J. Kowbel, *Cancer Res.*, 1979, **39**, 4412–4417.

6 Q. Wang, C. Cai, M. Wang, Q. Guo, B. Wang, W. Luo, Y. Wang, C. Zhang, L. Zhou and D. Zhang, *Materials*, 2018, **11**, 1004.

7 A. S. Sartape, A. M. Mandhare, V. V. Jadhav, P. D. Raut, M. A. Anuse and S. S. Kolekar, *Arabian J. Chem.*, 2017, **10**, S3229–S3238.

8 R. M. Silva, D. A. B. Barbosa, C. d. J. S. Mendonça, J. R. de Oliveira Lima, F. C. Silva, E. Longo, A. P. Maciel, C. W. de Araujo Paschoal and M. A. P. Almeida, *J. Phys. Chem. Solids*, 2016, **96**, 83–91.

9 F. D. Chequer, G. R. De Oliveira, E. A. Ferraz, J. C. Cardoso, M. B. Zanoni and D. P. de Oliveira, *Eco-Friendly Text. Dyeing Finish.*, 2013, **6**, 151–176.

10 M. Berradi, R. Hsissou, M. Khudhair, M. Assouag, O. Cherkaoui, A. El Bachiri and A. El Harfi, *Heliyon*, 2019, **5**, e02711.

11 F. Barancheshme and M. Munir, *Front. Microbiol.*, 2018, **8**, 2603.

12 C. Hayward, K. E. Ross, M. H. Brown and H. Whiley, *Pathogens*, 2020, **9**, 667.

13 M. Kaushik, S. Kumar, R. K. Kapoor and P. Gulati, *J. Med. Microbiol.*, 2019, **68**, 679–692.

14 T. Shindhal, P. Rakholiya, S. Varjani, A. Pandey, H. H. Ngo, W. Guo, H. Y. Ng and M. J. Taherzadeh, *Bioengineered*, 2021, **12**, 70–87.

15 A. Huang, M. Yan, J. Lin, L. Xu, H. Gong and H. Gong, *Int. J. Environ. Res. Public Health*, 2021, **18**, 4909.

16 A. A. Yaqoob, T. Parveen, K. Umar and M. N. Mohamad Ibrahim, *Water*, 2020, **12**, 495.

17 P. Rajasulochana and V. Preethy, *Resour.-Effic. Technol.*, 2016, **2**, 175–184.

18 H. Wang, T. Wang, B. Zhang, F. Li, B. Toure, I. B. Omosa, T. Chiramba, M. Abdel-Monem and M. Pradhan, *Clean: Soil, Air, Water*, 2014, **42**, 1029–1035.

19 Q. Mahmood, A. Pervez, B. S. Zeb, H. Zaffar, H. Yaqoob, M. Waseem and S. Afsheen, *BioMed Res. Int.*, 2013, **2013**, 796373.

20 P. Rajapaksha, A. Power, S. Chandra and J. Chapman, *Analyst*, 2018, **143**, 5629–5645.

21 C. M. Bezerra de Araujo, G. Filipe Oliveira do Nascimento, G. Rodrigues Bezerra da Costa, K. Santos da Silva, A. M. Salgueiro Baptisttella, M. Gomes Ghislandi and M. Alves da Motta Sobrinho, *Chem. Eng. Commun.*, 2019, **206**, 1375–1387.

22 K. Jain, A. S. Patel, V. P. Pardhi and S. J. S. Flora, *Molecules*, 2021, **26**, 1797.

23 N. A. Qasem, R. H. Mohammed and D. U. Lawal, *npj Clean Water*, 2021, **4**, 1–15.

24 S. De Gisi, G. Lofrano, M. Grassi and M. Notarnicola, *Sustainable Mater. Technol.*, 2016, **9**, 10–40.

25 K. Gupta and O. P. Khatri, *J. Colloid Interface Sci.*, 2017, **501**, 11–21.

26 F. Liu, S. Chung, G. Oh and T. S. Seo, *ACS Appl. Mater. Interfaces*, 2012, **4**, 922–927.

27 X. Zhou, Y. Guo, F. Zhao and G. Yu, *Acc. Chem. Res.*, 2019, **52**, 3244–3253.

28 O. Santiago, K. Walsh, B. Kele, E. Gardner and J. Chapman, *SpringerPlus*, 2016, **5**, 1–16.

29 S. Yu, H. Pang, S. Huang, H. Tang, S. Wang, M. Qiu, Z. Chen, H. Yang, G. Song and D. Fu, *Sci. Total Environ.*, 2021, **800**, 149662.

30 S. Yu, H. Tang, D. Zhang, S. Wang, M. Qiu, G. Song, D. Fu, B. Hu and X. Wang, *Sci. Total Environ.*, 2021, 152280.

31 S. Zhang, J. Wang, Y. Zhang, J. Ma, L. Huang, S. Yu, L. Chen, G. Song, M. Qiu and X. Wang, *Environ. Pollut.*, 2021, **291**, 118076.

32 H. Sadegh, G. A. Ali, V. K. Gupta, A. S. H. Makhlouf, R. Shahryari-Ghoshekandi, M. N. Nadagouda, M. Sillanpää and E. Megiel, *J. Nanostruct. Chem.*, 2017, 7, 1–14.

33 I. Ali, X. Mbianda, A. Burakov, E. Galunin, I. Burakova, E. Mkrtchyan, A. Tkachev and V. Grachev, *Environ. Int.*, 2019, **127**, 160–180.

34 F. Arias Arias, M. Guevara, T. Tene, P. Angamarca, R. Molina, A. Valarezo, O. Salguero, C. Vacacela Gomez, M. Arias and L. S. Caputi, *Nanomaterials*, 2020, **10**, 681.

35 R. J. Kadhim, F. H. Al-Ani, M. Al-Shaeli, Q. F. Alsalhy and A. Figoli, *Membranes*, 2020, **10**, 366.

36 E. Aliyev, U. Filiz, M. M. Khan, Y. J. Lee, C. Abetz and V. Abetz, *Nanomaterials*, 2019, **9**, 1180.

37 F. Perreault, A. F. De Faria, S. Nejati and M. Elimelech, *ACS Nano*, 2015, **9**, 7226–7236.

38 A. B. Alayande, M. Obaid and I. S. Kim, *Mater. Sci. Eng. Carbon*, 2020, **109**, 110596.

39 Y.-W. Wang, A. Cao, Y. Jiang, X. Zhang, J.-H. Liu, Y. Liu and H. Wang, *ACS Appl. Mater. Interfaces*, 2014, **6**, 2791–2798.

40 P. Rajapaksha, S. Cheeseman, S. Hombsch, B. J. Murdoch, S. Gangadoo, E. W. Blanch, Y. Truong, D. Cozzolino, C. F. McConville and R. J. Crawford, *ACS Appl. Bio Mater.*, 2019, **2**, 5687–5696.

41 J. L. Rufino, F. C. Fernandes, M. S. Ruy, H. R. Pezza and L. Pezza, *Ecletica Quim.*, 2010, **35**, 139–146.

42 J. Bayuo, M. A. Abukari and K. B. Pelig-Ba, *Appl. Water Sci.*, 2020, **10**, 1–6.

43 S. K. Shinde, D. P. Dubal, G. S. Ghodake, P. Gomez-Romero, S. Kim and V. J. Fulari, *RSC Adv.*, 2015, **5**, 30478–30484.

44 K. S. Siddiqi and A. Husen, *Biomater. Res.*, 2020, **24**, 1–15.

45 D. Piva, R. Piva, M. Rocha, J. Dias, O. Montedo, I. Malavazi and M. Morelli, *Adv. Powder Technol.*, 2017, **28**, 463–472.

46 G. Hitkari, S. Singh and G. Pandey, *Nano-Struct. Nano-Objects*, 2017, **12**, 1–9.

47 M. A. Atieh, O. Y. Bakather, B. Al-Tawbini, A. A. Bukhari, F. A. Abuilaiwi and M. B. Fettouhi, *Bioinorganic chemistry and applications*, 2010.

48 S. Kashyap, S. Mishra and S. K. Behera, *J. Nanopart.*, 2014, **2014**, 640281.

49 Z. Wang, S. Wu, J. Zhang, P. Chen, G. Yang, X. Zhou, Q. Zhang, Q. Yan and H. Zhang, *Nanoscale Res. Lett.*, 2012, **7**, 1–7.

50 M. Kumar, J. S. Chung and S. H. Hur, *Appl. Sci.*, 2019, **9**, 2925.

51 Y.-H. Chiu, T.-F. M. Chang, C.-Y. Chen, M. Sone and Y.-J. Hsu, *Catalysts*, 2019, **9**, 430.

52 Y.-C. Lee, J.-Y. Kim and H.-J. Shin, *Sep. Sci. Technol.*, 2013, **48**, 1093–1101.

53 Z. Feng, B. Su, D.-D. Xiao and L.-Y. Ye, *Journal of Information and Optimization Sciences*, 2017, **38**, 1197–1210.

54 C. Homsirikamol, N. Sunsandee, U. Pancharoen and K. Nootong, *Sep. Purif. Technol.*, 2016, **162**, 30–36.

55 M. J. Abadi, S. Nouri, R. Zhiani, H. Heydarzadeh and A. Motavalizadehkakhky, *Int. J. Ind. Chem.*, 2019, **10**, 291–300.

56 H. Zhu, T. Chen, J. Liu and D. Li, *RSC Adv.*, 2018, **8**, 2616–2621.

57 M. A. Ahmad, N. A. A. Puad and O. S. Bello, *Water Resour. Ind.*, 2014, **6**, 18–35.

58 Y. Gao, Y. Li, L. Zhang, H. Huang, J. Hu, S. M. Shah and X. Su, *J. Colloid Interface Sci.*, 2012, **368**, 540–546.

59 S. Banerjee and M. Chattopadhyaya, *Arabian J. Chem.*, 2017, **10**, S1629–S1638.

60 P. C. Bandara, J. V. D. Perez, E. T. Nadres, R. G. Nannapaneni, K. J. Krakowiak and D. F. Rodrigues, *ACS Appl. Polym. Mater.*, 2019, **1**, 2668–2679.

61 F. Younas, A. Mustafa, Z. U. R. Farooqi, X. Wang, S. Younas, W. Mohy-Ud-Din, M. Ashir Hameed, M. Mohsin Abrar, A. A. Maitlo and S. Noreen, *Water*, 2021, **13**, 215.

62 Y. Chen, Y. Zhang, C. Liu, A. Lu and W. Zhang, *Int. J. Photoenergy*, 2011, **2012**, 510158.

63 L. Yong, G. Zhanqi, J. Yuefei, H. Xiaobin, S. Cheng, Y. Shaogui, W. Lianhong, W. Qingeng and F. Die, *J. Hazard. Mater.*, 2015, **285**, 127–136.

64 L. Duan, L. Li, Z. Xu and W. Chen, *Environ. Sci.: Processes Impacts*, 2014, **16**, 1462–1468.

65 Y. Ho and G. McKay, *Process Saf. Environ. Prot.*, 1998, **76**, 332–340.

66 B. Mao, B. Sidhureddy, A. R. Thiruppathi, P. C. Wood and A. Chen, *New J. Chem.*, 2020, **44**, 4519–4528.

67 C. Zhao, J. Ma, Z. Li, H. Xia, H. Liu and Y. Yang, *RSC Adv.*, 2020, **10**, 5066–5076.

68 L. Lu, M. Liu, Y. Chen and Y. Luo, *R. Soc. Open Sci.*, 2021, **8**, 210336.

69 G. Liu, N. Wang, J. Zhou, A. Wang, J. Wang, R. Jin and H. Lv, *RSC Adv.*, 2015, **5**, 95857–95865.

70 Y. Yang, W. Yu, S. He, S. Yu, Y. Chen, L. Lu, Z. Shu, H. Cui, Y. Zhang and H. Jin, *Appl. Clay Sci.*, 2019, **168**, 304–311.

71 G. Ramesha, A. V. Kumara, H. Muralidhara and S. Sampath, *J. Colloid Interface Sci.*, 2011, **361**, 270–277.

72 B. Gao, P. Li, R. Yang, A. Li and H. Yang, *Sci. Rep.*, 2019, **9**, 1–13.

73 O. D. Agboola and N. U. Benson, *Front. Environ. Sci.*, 2021, **9**, 678574.

74 Y. Paz, *J. Phys.: Condens. Matter*, 2019, **31**, 503004.

75 J. Sahara, A. Naeema, M. Farooqa and S. Zareena, *Desalin. Water Treat.*, 2019, **164**, 228–239.

76 Y. Wang, C. Pan, W. Chu, A. K. Vipin and L. Sun, *Nanomaterials*, 2019, **9**, 439.

77 W. Guodong, S. Yongcai and L. Yongqiang, *RSC Adv.*, 2018, **8**, 21863–21870.

© 2022 The Author(s). Published by the Royal Society of Chemistry

Environ. Sci.: Adv., 2022, **1**, 456–469 | **469**